

RAD51 interconnects between DNA replication, DNA repair and immunity

Souparno Bhattacharya¹, Kalayarasan Srinivasan¹, Salim Abdisalaam¹, Fengtao Su¹, Prithvi Raj², Igor Dozmorov², Ritu Mishra¹, Edward K. Wakeland², Subroto Ghose³, Shibani Mukherjee³ and Aroumougame Asaithamby^{1,*}

¹Department of Radiation Oncology, University of Texas Southwestern Medical Center, Dallas, TX 75390, USA,

²Department of Immunology, University of Texas Southwestern Medical Center, Dallas, TX 75390, USA and

³Department of Molecular Psychiatry, University of Texas Southwestern Medical Center, Dallas, TX 75390, USA

Received August 06, 2016; Revised February 09, 2017; Editorial Decision February 12, 2017; Accepted February 13, 2017

ABSTRACT

RAD51, a multifunctional protein, plays a central role in DNA replication and homologous recombination repair, and is known to be involved in cancer development. We identified a novel role for RAD51 in innate immune response signaling. Defects in RAD51 lead to the accumulation of self-DNA in the cytoplasm, triggering a STING-mediated innate immune response after replication stress and DNA damage. In the absence of RAD51, the unprotected newly replicated genome is degraded by the exonuclease activity of MRE11, and the fragmented nascent DNA accumulates in the cytosol, initiating an innate immune response. Our data suggest that in addition to playing roles in homologous recombination-mediated DNA double-strand break repair and replication fork processing, RAD51 is also implicated in the suppression of innate immunity. Thus, our study reveals a previously uncharacterized role of RAD51 in initiating immune signaling, placing it at the hub of new interconnections between DNA replication, DNA repair, and immunity.

INTRODUCTION

DNA damage is a biological process that negatively impacts human health in many ways. Eukaryotic cells accrue DNA damage as a result of endogenous metabolic activities such as DNA replication, recombination errors or environmental exposures such as ionizing radiation, ultra-violet light and chemical mutagens. Alterations in the pathways involved in the processing of stalled or collapsed replication forks and DNA repair cause genome instability and chromosomal rearrangements that are hallmarks of cancer cells. RAD51 is one of multiple factors involved in faithful DNA replication, repair and recombination (1,2). Dur-

ing double-strand break (DSB) repair, RAD51 catalyzes the core reactions of homologous recombination (HR), including strand invasion into duplex DNA and the pairing of homologous DNA strands, enabling strand exchange (3). In addition to DSB repair, RAD51 also plays a role in various replication fork processes. RAD51 enables replication restart when a replication fork encounters DNA damage (1). Recent evidence indicates that RAD51 also prevents MRE11-mediated degradation of newly replicated genome after replication stress (4,5). Furthermore, RAD51 promotes cell survival following replication stress and prevents the accumulation of replication-associated DSBs (6) and genome instability.

Although germ-line mutations in the *Rad51* gene lead to embryonic death (7), a precisely regulated amount of RAD51 is crucial for normal cellular functions. Multiple human tumors exhibit varying expression levels of RAD51, deleterious mutations in the protein, or defects in other tumor suppressors, such as BRCA1, BRCA2, Fanconi anemia (FA) factors (8,9). Overexpression of RAD51 due to increased transcription reduces methylation and stabilization of the protein and may cause chromosomal amplifications, deletions, and translocations resulting in a loss of heterozygosity and aneuploidy. These events can lead to cancer development and progression to metastasis (10). In contrast, down-regulation of RAD51 has been reported in many tumors (11). Despite these reports, the precise mechanism by which RAD51 suppresses carcinogenesis is still elusive.

Carcinogenesis is a multistage process resulting from a cumulative malfunctioning of DNA replication, DSB repair and immune signaling. Chronic stimulation of the innate immune system can cause tumorigenesis (12,13). A number of studies have suggested that DNA repair and replication factors play a role in the innate immune response. For example, cells deficient in the DNA repair factor ataxia-telangiectasia mutated (ATM) were found to increase cytosolic self-DNA, leading to increased inflammation (14). Similarly, MRE11, a DSB sensor protein, recognizes cy-

*To whom correspondence should be addressed. Tel: +1 214 648 5175; Fax: +1 214 648 5995; Email: Asaithamby.Aroumougame@UTsouthwestern.edu

tosolic DNA and initiates innate immune response signaling (15). In addition, the DNA structure-specific endonuclease MUS81, which cleaves DNA structures at stalled replication forks, also mediates the stimulator of interferon genes (STING)-dependent activation of immune signaling (16). It was recently discovered that FA proteins are involved in cellular immunity (17). Moreover, RPA2 and RAD51 were shown to protect the cytosol from the accumulation of self-DNA (18). These findings indicate the involvement of DNA repair and replication factors in immunity in addition to their known DNA repair and replication functions. Importantly, mutations in the majority of these genes lead to cancer-prone disorders. However, whether defective RAD51 functions contribute to tumorigenesis through the activation of the innate immune system is still unknown.

We report a novel role of RAD51 in immunity in addition to its known functions in DSB repair and replication fork processing. We discovered that the down-regulation of RAD51 leads to the upregulation of innate immune response pathway genes upon DNA damage and replication stress induced by irradiation. In the absence of RAD51, the newly replicated genome is degraded by the exonuclease activity of MRE11. We also showed that these degraded nascent DNA fragments are exported to the cytoplasm, triggering innate immune response signaling. Our study reveals a previously unidentified role of RAD51 in triggering an innate immune response, placing this protein at the hub of new interconnections between DNA replication, DNA repair, and immunity.

MATERIALS AND METHODS

Cell lines and culture conditions

HT1080 cells were obtained from ATCC and maintained in Minimum Essential Medium (MEM) alpha supplemented with 10% fetal bovine serum, 100 mg/ml streptomycin sulfate and 100 U/ml penicillin. To establish the stable expression of cell cycle markers (HT1080-FUCCI), HT1080-EYFP-53BP1 cells (19) were transduced with lentivirus carrying G1 [mCherry-hCdt1(30/120)] and S/G2 [AmCyan-hGeminin(1/110)] phase markers. Stable HT1080-FUCCI cells were selected using zeocin (1 μ g/ml). To down-regulate the expression of RAD51, HT1080-FUCCI cells were transfected with a mammalian expression plasmid containing tetracycline-inducible Rad51 shRNA (20). Stable lines were selected using hygromycin (75 μ g/ml). To down-regulate RAD51 protein levels, cells were cultured in the presence of doxycycline (DOX, 1 μ g/ml) for 72 h. MCF10A cells stably expressing scrambled and Rad51 shRNA were kind gift from Dr Shiaw-Yih Lin (MD Anderson Cancer center) and were maintained in mammary epithelial basal medium (LONZA, CC-3151) as described previously (21). 4T1 cells were maintained as described previously (22). To down-regulate the expression of RAD51, 4T1 cells were transfected with a mammalian expression plasmid containing tetracycline-inducible Rad51 shRNA and selected using puromycin (1 μ g/ml). All cells were maintained at 37°C in a humidified 5% CO₂ incubator.

Irradiation and dosimetry

DNA lesions and replication stress were induced by exposing the cells to high-LET iron (Fe) particles generated at the NASA Space Radiation Laboratory in Brookhaven National Laboratory, Long Island, NY. The energy of the used Fe-particles was 1 GeV/nucleon and the dose rate ranged from 50 to 200 cGy/min. The linear energy transfer (LET) of the Fe-particles was 150 keV/ μ m. The residual ranges of the beams were determined before each experiment and used to calculate the track-averaged LET values (23).

Drugs and antibodies

The following reagents were used: Doxycycline (Sigma-Aldrich, D9891), MRE11 inhibitor [5-(4-hydroxybenzylidene)-2-iminothiazolidin-4-one, (Sigma-Aldrich, M9948)], IdU (Sigma-Aldrich, I7125), CldU (Sigma-Aldrich, C6891) and Histone deacetylase inhibitor, suberoylanilide hydroxamic acid (Tocris Biosciences, 4652). Mouse monoclonal anti- γ H2AX (JBW301; EMD Millipore, 07-164), rabbit polyclonal anti-RAD51 (H-92; Santa Cruz, sc-8349), rabbit polyclonal anti-STING (Novus Biologicals, 2-24683), anti-phospho-STING (Ser366; Cell Signaling, 85735), rabbit monoclonal anti-phospho-TBK1 (Ser172; D52C2; Cell Signaling, 5483), rabbit polyclonal anti-phospho-STAT3 (Tyr705; Cell Signaling, 9131), rabbit monoclonal anti-CASPASE-3 (8G10; Cell Signaling, 9665), mouse monoclonal anti-PARP1 (F2; Santa Cruz, 8007), mouse monoclonal anti- γ -Tubulin (GTU-88; Sigma-Aldrich, T6557), mouse monoclonal anti-BrdU (B44; BD Biosciences, 347580) and rat monoclonal anti-BrdU (BU1/75-ICR1; Novus Biologicals, NB500-169) antibodies. Fluorescent conjugated secondary antibodies Alexa488, Alexa555, Alexa633, were purchased from Molecular Probes (Invitrogen).

Drug treatment

For inducible depletion of RAD51, HT1080 and 4T1 cells were grown in presence of 1 μ g/ml doxycycline for 72 h and then exposed to radiation. For the pharmacological depletion of RAD51, HT1080 cells were grown in presence of 2.0 μ M suberoylanilide hydroxamic acid (SAHA) for 36 h and then allowed to recover for an additional 12 h before irradiation. For the MRE11 inhibitor treatment, cells were treated with 25 μ M mirin 1 h prior to irradiation and the cells were maintained in mirin-containing medium until the end of the experiment.

Indirect immunofluorescence staining

About 5×10^4 cells were seeded in a six-well plate containing cover glasses, incubated for 24 h, treated with doxycycline (DOX, 1 μ g/ml) for 72 h, and exposed to 1–2 Gy Fe-particles. Cells were fixed with 4% paraformaldehyde at room temperature for 20 min at different post-IR times and treated for indirect immunofluorescence as described previously (19). For the detection of RAD51 foci, cells were washed three times in PBS and incubated in extraction buffer (10 mM HEPES, pH 7.4, 300 mM sucrose, 100 mM NaCl, 3 mM MgCl₂, 0.1% Triton X-100) on ice

for 10 min before fixation. For immunostaining, cells were permeabilized in Triton X-100 (0.5% in PBS) on ice for 5 min, washed three times with PBS, incubated in blocking solution (5% goat serum in PBS) at room temperature for 60 min, and incubated with primary antibodies (diluted in 5% goat serum) at room temperature for another 3 h. Subsequently, cells were washed with 1% BSA in PBS, incubated with appropriate secondary antibodies (1:1000 in 2.5% goat serum, 1% BSA, and PBS) at room temperature for 60 min, washed five times with 1% BSA, and mounted with mounting medium containing DAPI (4',6-diamidino-2-phenylindole, Vectashield).

For cytoplasmic BrdU detection, exponentially grown cells were labeled with 20 μ M BrdU for 18–20 h in regular growth medium, replaced with regular medium without BrdU, irradiated and fixed with 80% methanol (in PBS) on ice for 20 min. Fixed cells were washed three times with cold PBS, incubated in blocking solution (5% goat serum in PBS) at room temperature for 1 h, and treated with anti-BrdU antibody (mouse) overnight at 4°C. Cells were washed with 1% BSA in PBS, incubated with the Alexa 555 secondary antibody at room temperature for 1 h, washed five times with 1% BSA, and mounted with mounting medium containing DAPI (Vectashield).

Image acquisition and foci counting

Images were captured using a LSM 510 Meta laser scanning confocal microscope with a 63 \times 1.4 NA Plan-Apochromat oil immersion objective. Images were taken at z-sections (15–20 sections) of 0.35- μ m intervals using 405-nm (DAPI), 457-nm (AmCyan), 488-nm (Alexa 488), 514-nm (EYFP), 543-nm (mCherry/Alexa 555) and 633-nm (Alexa 633) lasers. The tube current of the 488-nm argon laser was set at 6.1 A. The laser power was typically set to 3–5% transmission with the pinhole opened at 1 Airy unit. To count γ H2AX foci in different cell cycle phases, we developed an algorithm in MatLab (MathWorks, MA) and used it to count foci in G1 and S/G2 phases. The quantification of foci was conducted from images of 100–200 cells for each time point from three to four independent experiments (19).

Whole-cell extract preparation and western blotting

Whole-cell extracts were prepared in radio-immunoprecipitation assay (RIPA) buffer according to a published procedure (24). The protein concentration was measured by the bicinchoninic acid (BCA) assay. Aliquots containing 50–150 μ g protein were resolved by 8–15% SDS-PAGE, transferred onto nitrocellulose or PVDF membrane, and incubated with the indicated antibodies either at room temperature for 4 h or overnight at 4°C (4,25).

Sub-cellular fractionation

The cytoplasmic extract was isolated following a previously published methodology (14). Briefly, cells were re-suspended in 10 mM of HEPES (pH 7.9), 10 mM KCl, 1.5 mM MgCl₂, 0.34 M sucrose, 10% glycerol, 0.1% Triton X-100, protease inhibitors cocktail (Roche, 11836170001),

and incubated on ice for 10 min. The nuclei were separated from the cytoplasmic extract by low-speed centrifugation (1500 relative centrifugal force) at 4°C for 5 min. The supernatant containing the cytosolic extract was either immediately used for single-strand (ssDNA) and double-strand (dsDNA) DNA quantification or stored at –80°C until use.

Quantification of cytosolic single-strand (ssDNA) and double-strand (dsDNA) DNA

ssDNA and dsDNA in the cytosolic fractions were quantified using Quant-iT OliGreen and PicoGreen Assay Kits (O11492 and P7589 kits, respectively; Invitrogen). Briefly, black 96-well plates (Phenix Research Product, MPG-655076) were first loaded with 98 μ l of 1 \times trypsin–EDTA in each well and then with 2 μ l of cytosolic extracts. Subsequently, 100 μ l of 2 \times OliGreen or PicoGreen dye was added into each well. This mixture was incubated in the dark for 5 min, and the fluorescence intensity was measured at an excitation wavelength of 480 nm and an emission wavelength of 520 nm using a Spectrofluorometer (Perkin Elmer 2030 Multilabel Reader, Victor X3). Standard curves were generated for each experiment using standard M13 primer and Lambda DNA for ssDNA and dsDNA diluted in cytosolic extraction buffer, respectively. The final ssDNA and dsDNA concentration was calculated by normalizing against cytosolic protein concentration and presented as fold change relative to sham treated controls or picogram DNA per microgram of cytosolic protein.

Microarray

Total RNA was isolated from mock-treated and irradiated cells using the Qiagen RNeasy kit (217004, Qiagen), according to manufacturer's instructions. The RNA quality was determined using the Experion system (Bio Rad). Samples were processed and hybridized to Illumina Human HT12v4 arrays (Illumina, Inc.) using standard Illumina protocols. The slides were scanned on an Illumina Beadstation (Illumina, Inc.; Genomics Core, UT Southwestern Medical Center).

Microarray data processing and pathway analysis

The methods for data normalization and analysis were based on the use of 'internal standards' (26) that characterize some aspects of the system's behavior such as technical variability (27,28). The comparison between these methods with other normalization and analysis procedures was previously published (29). The two-step normalization procedure and the associative analysis functions were implemented in MatLab (Mathworks, MA, USA) and are available from the authors upon request. These algorithms can also be obtained from an R package *diffGeneAnalysis*, available as part of Bioconductor packages (<http://www.bioconductor.org/packages/2.5/bioc/html/diffGeneAnalysis.html>). Heatmaps were generated with the Spotfire Decision Site 9 (TIBCO, Palo Alto, CA, USA) with gene subsets created from the list of significant genes. The accession number for the newly reported microarray data is NCBI GEO series accession number GSE95050.

Quantitative real-time polymerase chain reaction (qRT-PCR)

cDNA was synthesized from 1 to 3 μg of RNA using SuperScript III Reverse Transcriptase (18-080-051 Fischer Scientific) in a total volume of 20 μl , according to manufacturer's instructions. The cDNA was subjected to qRT-PCR for a number of genes using the primer sets (Supplementary Table S1), CFX96 Touch Real-Time PCR Detection System (Bio Rad) and iTaq Universal SYBR Green Supermix (Bio Rad, 1725121), according to manufacturer's instructions. The relative gene expression was determined by the $\Delta\Delta\text{CT}$ method. The difference in cycle times ΔCT was determined as the difference between the tested gene of interest and the reference housekeeping β -actin gene. The $\Delta\Delta\text{CT}$ was obtained by finding the difference between the groups. The fold change (FC) was calculated as $\text{FC} = 2^{-\Delta\Delta\text{CT}}$. All primers were purchased from Invitrogen. qRT-PCR assays were carried out in triplicates for each sample. The mean value was used for the calculation of the mRNA expression levels and presented as fold change relative to respective sham treated controls.

DNA fiber assay

A DNA fiber assay was performed as described previously (4,30). Briefly, 2.5×10^5 cells were labeled with IdU (150 μM) for 30 min, washed four times with warm PBS, labeled with or without CldU, treated with and without radiation (1 Gy), and recovered for either 30 min or 5 h. After three washes with warm PBS, both labeled and unlabeled cells were trypsinized and mixed at a 1:15 ratio (labeled:unlabeled). Both cell types were lysed on a clean glass slide in 20 μl of lysis buffer (0.5% SDS, 50 mM EDTA, and 200 mM Tris-HCl pH7.4) for 8 min; slides were tilted slightly ($\sim 15^\circ$ angle) to help the DNA spread slowly. Subsequently, slides were immunostained with anti-BrdU antibodies, and the DNA fiber lengths were measured using Axiovision Software.

Cell survival assay

Cell survival was measured using a colony formation assay (31). About 1000–20 000 cells were seeded in triplicates in 6-well plates, incubated for 6–8 h before IR, and irradiated with 0.5 Gy. Immediately after irradiation, cells were allowed to form colonies for 8–10 days. Colonies were washed once with $1 \times$ PBS, fixed with 70% ethanol for 10 min, and stained with 0.5% crystal violet dissolved in 25% methanol and 75% water. Colonies composed of > 50 cells were scored as having grown from a single surviving cell. Survival graphs were generated from three replicate wells with colony numbers normalized to sham-treated controls.

Metaphase spreads preparation

Chromosome aberrations were carried out as described previously (31). Sixteen hours after 1 Gy irradiation, chromosome preparations were made by accumulating metaphases in the presence of 0.1 mg/ml colcemid (Irvine Scientific) for 6 h. In the case of experiments with mirin, the medium was replaced with either fresh medium containing 25 μM

mirin or DMSO 1 h before radiation. The cells were maintained in mirin-containing medium until the end of the experiment. Chromosome images were taken using an Olympus microscope (100 \times objective) equipped with an Image Spot camera (Spot Imaging Solutions). Chromosome aberrations were scored as described previously (31).

Statistical analysis

Data are expressed as means \pm SEM or STDEV of three to four independent experiments. The Student's *t* test was performed on all values and $P < 0.05$ was considered statistically significant. GraphPad Prism (version 7.0) was used to create the graphs. SigmaPlot (version 12.5) was used to calculate foci dissolution kinetics.

RESULTS

RAD51-depletion leads to the up-regulation of innate immune response genes

It was previously shown that RAD51 plays a central role in homologous recombination (HR)-mediated DNA double-strand break (DSB) repair and replication fork processing. To gain new insight into the function of RAD51 outside DSB repair and replication fork processing, we conducted gene expression profiling of RAD51-proficient and -depleted cells (Figure 1A) by microarray after DNA damage and replication stress. We used high-linear energy transfer radiation to induce both DNA lesions and replication stress (30,31). We found that expression levels of a number of genes were significantly ($P < 0.05$) altered in irradiated RAD51-proficient and -depleted cells as compared to corresponding mock-treated cells (Supplementary Figure S1A). Subsequently, we performed gene ontology analysis on differentially expressed gene sets using the Ingenuity Pathway Analysis (IPA) software. Our data indicated that the expression of genes known to function in DNA replication, recombination, and repair, and in the cell cycle were significantly altered in both irradiated RAD51-proficient and -depleted cells as compared to their corresponding mock-irradiated cells (data not shown). Interestingly, IPA analysis revealed that the expression of many genes with known functions in innate immunity were up-regulated significantly in irradiated RAD51-depleted cells as compared with irradiated RAD51-proficient cells (Figure 1B and C and Supplementary Figure S1B). These results revealed that the depletion of RAD51 results in the up-regulation of innate immune response genes upon irradiation.

Subsequently, we validated a set of six genes that showed elevated expression patterns in the microarray by quantitative real-time polymerase chain reaction (qRT-PCR), using mRNA purified from mock-treated and irradiated RAD51-proficient and -depleted cells. Similarly to the microarray results, expression levels of IL-6, CSF2, CXCR4, TNF- α , CMKLR1 and TLR9 expression were 12, 10, 5, 3.2, 6 and 3.2 folds, respectively significantly higher in irradiated RAD51-depleted cells than in irradiated RAD51-proficient cells ($P < 0.05$ – 0.008 ; Figure 1D–I). Taken together, these results clearly indicate that the depletion of RAD51 leads to the up-regulation of many genes involved in the innate immune response pathway following irradiation.

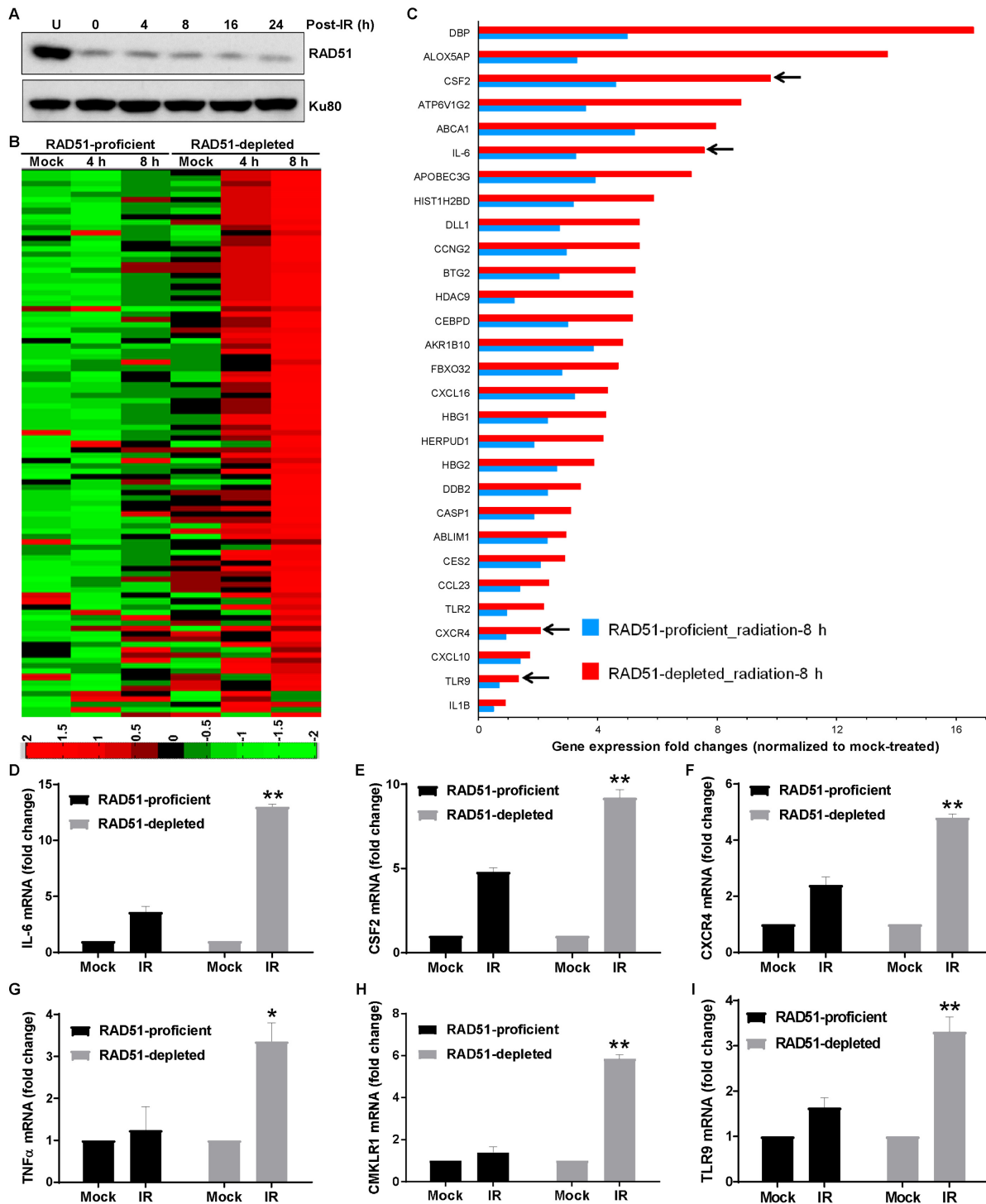


Figure 1. Depletion of RAD51 up-regulates innate immune response pathway genes. (A) shRNA-mediated depletion of RAD51 expression in HT1080 cells: HT1080 cells stably integrating tetracycline-inducible Rad51 shRNA were treated with 1 μ g/ml doxycycline (DOX) for 72 h. Subsequently, cells were exposed to 1 Gy of radiation (IR), collected at pre-established time points after irradiation. Total cell lysates (50 μ g) were separated on 8% SDS-PAGE and probed with anti-RAD51 and anti-Ku80 (loading control) antibodies. U- without DOX treatment. (B) Heat map of significantly altered innate immune response pathway genes in RAD51-proficient and -depleted cells 4 and 8 h after irradiation. (C) Graph shows fold changes in gene expression in irradiated (8 h) cells normalized to gene expression values in corresponding mock-treated cells. Exponentially growing RAD51-proficient and -depleted HT1080 cells were either mock-treated or irradiated with 1 Gy. Total RNA was prepared at indicated times after irradiation and analyzed for gene expression profiling using Human HT12v4 Arrays. The heat map for innate immune response network genes was generated with gene subsets created from the list of significant innate immune response genes using Spotfire Decision Site 9. (D–I) Differences in expression levels of innate immune response pathway genes measured by quantitative real-time polymerase chain reaction (qRT-PCR): RAD51-proficient and -depleted HT1080 cells were irradiated (IR) with 1 Gy and total RNA was prepared 8 h after irradiation. mRNAs were converted into cDNA and the levels of IL-6 (D), CSF2 (E), CXCR4 (F), TNF- α (G), CMKLR1 (H) and TLR9 (I) mRNA were quantified by qRT-PCR. Error bars represent the SEM from three independent experiments; * P < 0.05; ** P < 0.01.

RAD51-depleted cells accumulate elevated levels of cytosolic DNA

The mechanism underlying the up-regulation of innate immune response pathway genes in RAD51-depleted cells upon irradiation is unknown. An innate immune response is known to be triggered by cytosolic DNA (32). To identify whether the up-regulation of innate immune response pathway genes in response to irradiation in RAD51-depleted cells is due to the elevated amount of cytosolic DNA, we quantified single- (ssDNA) and double-strand (dsDNA) DNA in the cytoplasmic fractions of RAD51-proficient and -depleted cells at different intervals after irradiation. The amount of cytosolic ssDNA (12.83 ± 3.51 and 12.91 ± 3.86 pg/ μ g protein in mock and irradiated cells, respectively; Figure 2A) and dsDNA (4.0 ± 0.03 and 3.95 ± 0.42 pg/ μ g protein in mock and irradiated cells, respectively; Figure 2B) was similar in mock and irradiated RAD51-proficient cells. In contrast, the amount of cytosolic ssDNA (12.19 ± 3.18 and 19.91 ± 3.05 pg/ μ g protein in mock and irradiated cells, respectively; $P = 0.0006$; Figure 2A) and dsDNA (4.4 ± 0.38 and 9.37 ± 0.67 pg/ μ g protein in mock and irradiated cells, respectively; $P = 0.0004$; Figure 2B) was significantly higher in RAD51-depleted cells as compared to RAD51-proficient cells 8 h after irradiation. These results clearly demonstrate that the depletion of RAD51 leads to elevated levels of cytosolic DNA in response to irradiation.

To further rule out the possibility that the elevated levels of cytosolic DNA and activation of innate immune response genes in irradiated RAD51-depleted cells are not due to cells undergoing apoptosis, we checked the level of cleaved products of CASPASE-3 and PARP-1 by western blotting at different times after radiation exposure. Cleaved CASPASE-3 and fragmented PARP-1 are recognized biomarkers for cells undergoing apoptosis (33,34). Cleaved PARP-1 and CASPASE-3 levels were not different between irradiated RAD51-proficient and -depleted cells at any time after irradiation (Figure 2C). Thus, these results indicate that the elevated level of cytosolic DNA in RAD51-depleted cells upon irradiation is not due to cells undergoing apoptosis.

Next, we verified whether the accumulation of cytosolic DNA is unique to RAD51-depletion in HT1080 cells or it can also occur in other cell types lacking RAD51. First, we used a previously published MCF10A cells stably expressing scrambled (shscr) and Rad51-specific shRNA (21) and examined the levels of cytosolic DNA (Figure 2f, inset). As in RAD51 depleted HT1080 cells, the amount of cytosolic ssDNA and dsDNA (36.75 ± 5.01 and 5.63 ± 0.51 pg/ μ g protein ssDNA and dsDNA, respectively; $P < 0.002$ – 0.0002) was significantly higher in irradiated MCF10A-shRad51 cells relative to irradiated MCF10A-shscr cells (22.7 ± 3.37 and 3.54 ± 0.66 pg/ μ g protein ssDNA and dsDNA, respectively; Figure 2D–E). Importantly, elevated levels of cytosolic DNA correlated well with the increased expression of innate immune response genes (TNF- α , TLR9 and CMKLR1) in irradiated RAD51-depleted cells ($P < 0.002$ – 0.0001 ; Figure 2F). Thus, these results confirmed that the observation on the activation of innate immune response in RAD51-depleted cells upon irradiation is not limited to one cell type.

To further confirm that the role of RAD51 in innate immunity is not limited to human cells, we performed experiments in mouse mammary carcinoma cells (4T1) stably expressing tetracycline inducible mouse shRad51. Similar to human cells, the cytosolic ssDNA levels were significantly elevated in 4T1-depleted cells 8 h after irradiation (12.96 ± 0.75 and 21.1 ± 1.1 pg/ μ g protein in mock and irradiated cells, respectively, $P < 0.0005$) as compared with irradiated RAD51-proficient 4T1 cells (18.44 ± 2.61 and 17.84 ± 0.76 pg/ μ g protein, in mock and irradiated cells, respectively, Figure 2G–H). Similarly, the cytosolic dsDNA levels were also significantly elevated in irradiated 4T1-depleted cells (4.79 ± 0.45 and 7.11 ± 0.39 pg/ μ g protein in mock and irradiated cells, respectively, $P < 0.02$) as compared with irradiated RAD51-proficient 4T1 cells (6.99 ± 0.88 and 6.96 ± 0.29 pg/ μ g protein in mock and irradiated cells, respectively, Figure 2G–H). Importantly, elevated levels of cytosolic DNA correlated well with the increased levels of innate immune response genes (IL-6, CSF2, TLR9 and TNF- α) expression in 4T1-depleted cells upon irradiation ($P < 0.007$ – 0.0006 ; Figure 2I). Thus, RAD51 is involved in the suppression of cytosolic DNA accumulation in response to radiation in different mammalian cell types.

In addition to the genetic depletion of RAD51 in different mammalian cells, we pharmacologically down-regulated RAD51 levels in HT1080 cells using SAHA (35). As reported previously (35), the treatment of HT1080 cells with SAHA reduced the levels of RAD51 expression in HT1080 cells (Figure 2L, inset). Subsequently, we measured the levels of both cytosolic DNA and expression of innate immune response genes after irradiation. Similarly to the genetic knock-down of RAD51, SAHA treated irradiated cells showed increased amount of ssDNA (37.2 ± 4.17 and 58.07 ± 5.9 pg/ μ g protein in SAHA treated control and irradiated cells, respectively; $P < 0.002$) and dsDNA (8.6 ± 0.78 and 12.6 ± 0.87 pg/ μ g protein in SAHA treated control and irradiated cells, respectively; $P < 0.007$) relative to cytoplasmic ssDNA and dsDNA levels in sham treated HT1080 cells exposed to radiation (12.91 ± 3.86 and 3.95 ± 0.42 pg/ μ g protein ssDNA and dsDNA, respectively; Figure 2J–K). Elevated levels of cytosolic DNA correlated with the increased levels of innate immune response gene (IL-6, CSF2, TLR9 and TNF- α) expression in SAHA-treated HT1080 cells upon irradiation relative to SAHA treated control cells ($P < 0.02$ – 0.0001 ; Figure 2I). Overall, RAD51 is involved in the suppression of innate immune response upon irradiation.

Nuclear-derived self-DNA accumulates in the cytosol of RAD51-depleted cells

To identify the source of cytoplasmic DNA and to distinguish the cell-cycle-dependent accumulation of cytosolic DNA, we labeled the genomic DNA of HT1080-FUCCI cells with 5-bromo-2'-deoxyuridine (BrdU) for 18–20 h, followed by irradiation. Subsequently, we immunostained the cells with anti-BrdU antibodies under non-denaturing conditions and quantified the mean BrdU fluorescent intensity (MFI) per cell. Quantification of cell cycle specific cytoplasmic BrdU intensity (Figure 3A) showed that the cytoplasmic BrdU intensity was comparable between G1 and S/G2

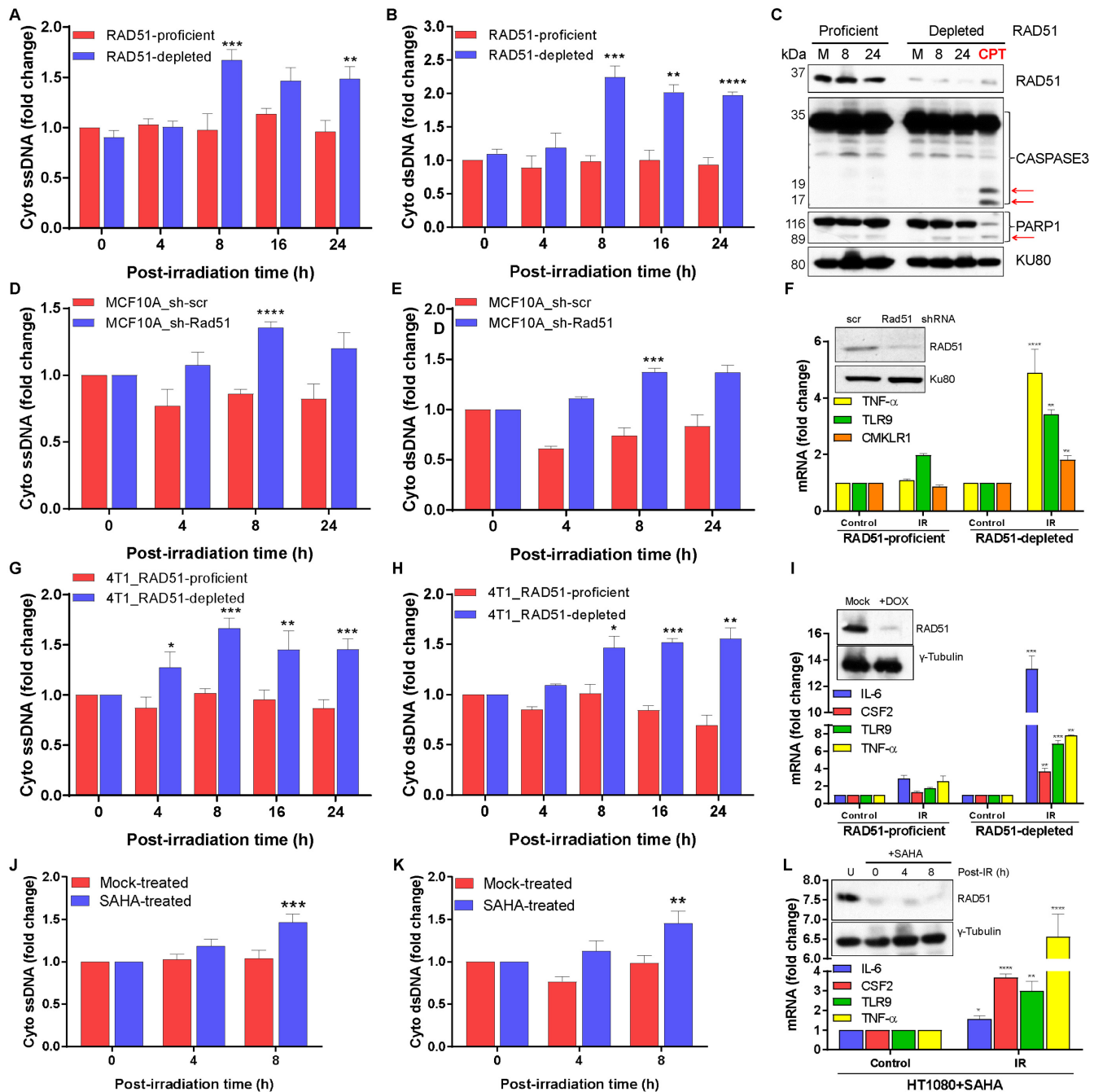


Figure 2. Excessive DNA accumulates in the cytosol of RAD51-depleted cells. (A and B) Quantification of single-strand (ssDNA) and double-strand (dsDNA) DNA in the cytosol (cyto): RAD51-proficient and -depleted HT1080 cells were irradiated with 2 Gy and were harvested at the indicated times. Subsequently, cells underwent sub-cellular fractionation and the amount of cytosolic ssDNA (A) and dsDNA (B) were quantified using OliGreen and PicoGreen Quant-iT reagents, respectively. Bars represent fold changes in the cytoplasmic DNA concentration relative to RAD51-proficient mock-treated samples. Error bars represent the SEM from four independent experiments; ** $P < 0.01$; *** $P < 0.001$; **** $P < 0.0001$. (C) Western blots show lack of apoptosis-mediated cleavage of CASPASE-3 and PARP-1 in RAD51-proficient and -depleted HT1080 cells following irradiation: RAD51-proficient and -depleted HT1080 cells were exposed to 2 Gy of radiation and cells were harvested at indicated time points after irradiation. Total cell lysates (50–100 μ g) were separated on 8–15% SDS-PAGE and probed with anti-CASPASE-3, anti-PARP1, and anti-Ku80 (loading control) antibodies. RAD51-depleted HT1080 cells treated with 1 μ M camptothecin (CPT) for 18 h was used as a positive control for apoptosis. M-mock-irradiated; arrows indicate cleaved CASPASE-3/PARP-1. (D–L) Accumulation of ssDNA and dsDNA in the cytoplasm, and expression of innate immune response genes in RAD51-proficient and -depleted MCF10A (D–F), 4T1 (G–I) and HT1080+SAHA cells (J–L). The bars represent the fold changes in the cytoplasmic DNA concentration and immune response genes relative to respective mock-treated controls. Cells were either mock- or exposed to 2 Gy of radiation (IR), cytosolic fraction and total RNA was prepared at 8 (MCF10A), 16 (HT1080+SAHA) and 24 (4T1) h after irradiation, and ssDNA, dsDNA and the levels of innate immune response genes were quantified as described in materials and methods. Error bars represent the STDEV from four different experiments from two independent sets; * $P < 0.05$; ** $P < 0.01$; *** $P < 0.001$; **** $P < 0.0001$. SAHA-suberoylanilide hydroxamic acid; U- without SAHA treatment.

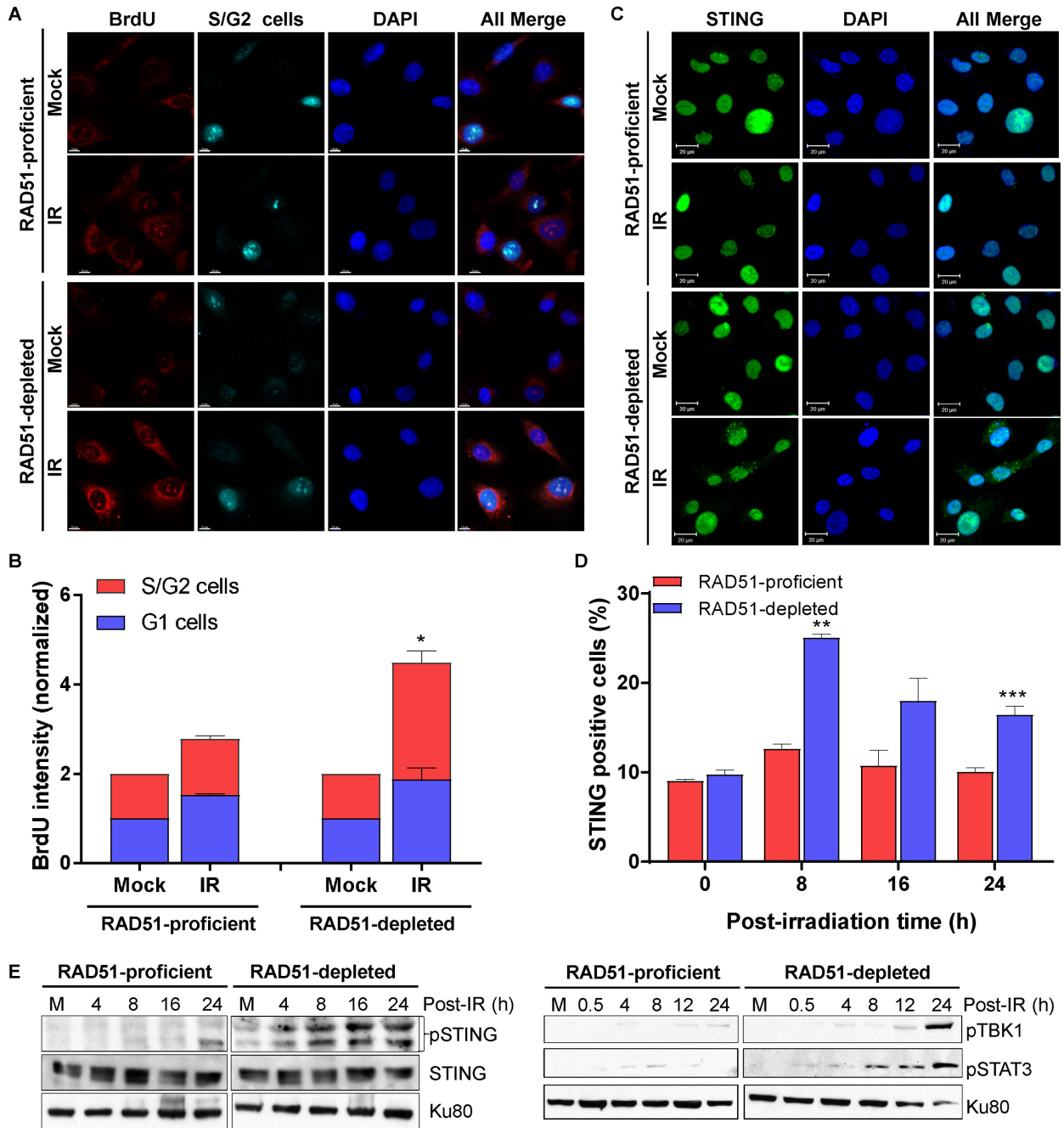


Figure 3. Accumulation of nuclear-derived DNA in the cytosol activates STING in RAD51-depleted cells. (A and B) Representative images show accumulation of nuclear-derived DNA in the cytoplasm of mock- and irradiated (IR) G1 and S/G2 phase RAD51-proficient and -depleted cells (A). Graph shows quantification of the cell cycle-dependent cytoplasmic BrdU signal normalized to mock-treated RAD51-proficient samples (B). RAD51-proficient and -depleted HT1080-FUCCI cells were labeled with BrdU for 18–20 h, irradiated with 2 Gy and fixed with ice cold 80% methanol in PBS 8 h after irradiation. Cells were immunostained with an anti-BrdU antibody under non-denaturing conditions. Subsequently, cells were imaged using a LSM510 confocal microscope, and the mean fluorescence BrdU signal in the cytoplasm of G1 and S/G2 phase cells was quantified using ZEN 2009 (version 6.0.0303) Software (Carl Zeiss, Jena, Germany). Bars represent mean cytoplasmic BrdU intensity per cell relative to respective control G1 and S/G2 cells. More than 150 cells were used for quantification in each condition. Error bars represent the STDEV from two-four independent experiments; Scale bars are 10 μ m; * P < 0.05. (C and D) Representative images show STING clustering in the cytoplasm of mock- and irradiated RAD51-proficient and -depleted cells 8 h after irradiation (C). Quantification of percentage of cells with STING clustering signal relative to the total number of counted cells (D). RAD51-proficient and -depleted HT1080 cells were irradiated with 2 Gy and fixed with 4% PFA at indicated times after irradiation. Subsequently, cells were immunostained with an anti-STING antibody, imaged using a LSM510 confocal microscope; the STING clustering signal in the cytoplasm was quantified using Imaris Software (Bitplane). More than 200 cells were used for quantification in each condition. Error bars represent the STDEV from three independent experiments; Scale bars are 20 μ m; ** P < 0.01; *** P < 0.001. (E) Representative Western blots show phosphorylation of STING, TBK, and STAT3 in RAD51-proficient and -depleted cells after irradiation. RAD51-proficient and -depleted HT1080 cells were irradiated with 2 Gy radiation and harvested at the indicated times. Total cell lysates (100–150 μ g) were separated on 8–10% SDS-PAGE and probed with the indicated antibodies and the anti-Ku80 antibody (loading control).

cells in both non-irradiated RAD51-proficient and (3.2 ± 0.38 and 4.28 ± 0.09 MFI per G1 and S/G2 cell, respectively) and RAD51-depleted cells (5.0 ± 0.83 and 5.11 ± 0.08 MFI per G1 and S/G2 cell, respectively, Figure 3B). We observed a slight increase in the cytoplasmic BrdU intensity after radiation in RAD51-proficient cells, but there were no significant difference in the cytoplasmic BrdU intensity between G1 and S/G2 cells after irradiation (5.08 ± 0.18 and 5.40 ± 0.15 MFI per G1 and S/G2 cell, respectively) cells (Figure 3B). In contrast, we observed a highly significant increase in cytoplasmic BrdU intensity in RAD51-depleted cells after radiation relative to irradiated RAD51-proficient cells (5.24 ± 0.02 and 10.92 ± 0.08 MFI per cell, $P < 0.0001$). Furthermore, the cytoplasmic BrdU fluorescent intensity in irradiated RAD51-depleted S/G2 cells (12.27 ± 0.06 MFI per cell; $P < 0.0006$) was significantly higher relative to irradiated RAD51-proficient S/G2 (5.41 ± 0.14 MFI per cell) cells (Figure 3B). More importantly, cytoplasmic BrdU fluorescent intensity significantly increased in RAD51-depleted S/G2 (12.27 ± 0.06 MFI per cell) cells than in G1 cells (9.57 ± 0.09 MFI per cell; $P < 0.001$) after irradiation (Figure 3B). Thus, cytoplasmic DNA is derived from the nuclear DNA and RAD51-depleted S/G2 cells harbor a major fraction of cytosolic self-DNA upon irradiation.

Cytosolic self-DNA activates the stimulator of interferon gene (STING) signaling in RAD51-depleted cells

Evidence suggests that the innate immune response resulting from cytoplasmic nucleic acid is mediated by STING activation, including clustering and phosphorylation (14,15). It has been reported that activated STING forms higher order clusters (36). To verify whether the presence of self-DNA in the cytoplasm triggers STING clustering, we conducted immunostaining with anti-STING antibody (Figure 3C). No significant changes in STING clustering were observed in both mock- and irradiated RAD51-proficient cell percentages (Figure 3D). In contrast, STING clustering percentages were significantly higher in irradiated RAD51-depleted cells ($P < 0.002$) than in irradiated RAD51-proficient cells (Figure 3D). To further confirm whether the presence of self-DNA in the cytoplasm activates STING, we evaluated STING phosphorylation by Western blotting. We detected strong STING phosphorylation in RAD51-depleted cells as early as 4 h after irradiation which further increased at 8 h and remained stable at later time points (Figure 3E, left panel). In contrast, the level of STING phosphorylation was much delayed and visibly weak in irradiated RAD51-proficient cells (Figure 3E, left panel). Thus, the accumulation of self-DNA in the cytosol activates STING in cells lacking RAD51 upon irradiation.

Tank binding kinase-1 (TBK1) is known to transmit immune signals downstream of STING in response to cytoplasmic DNA (37,38). To determine whether an increased STING activity in RAD51-depleted cells stimulates TBK1 activity, we monitored TBK1 phosphorylation by Western blotting. We detected TBK1 phosphorylation as early as 8 h and thereafter observed increased phosphorylation levels in irradiated RAD51-depleted cells (Figure 3E, right panel). In contrast, RAD51-proficient cells only showed

a minimal increase in TBK1 phosphorylation after irradiation. Furthermore, TBK1 activates STAT3 leading to the upregulation of IL-6 (39). To further dissect the innate immune signaling network downstream of the STING-TBK1 axis, we verified STAT3 phosphorylation in RAD51-proficient and -depleted cells after irradiation. We detected low levels of STAT3 phosphorylation in irradiated RAD51-proficient cells (Figure 3E, right panel). In contrast, STAT3 phosphorylation was higher in irradiated RAD51-depleted cells than in irradiated RAD51-proficient cells (Figure 3E). Thus, the activation of STING-TBK1 leads to the activation of STAT3 in response to self-DNA in RAD51-depleted cells. Overall, these results revealed that the presence of self-DNA in the cytoplasm initiates STING-mediated innate immune response signaling.

RAD51 blocks the MRE11-mediated degradation of nascent DNA strands in response to DNA damage

Nuclear DNA accumulates in the cytoplasm as a result of DNA damage, replication stress (40,41), or replication intermediates (42). RAD51 has been implicated in replication fork progression, efficient restart, and stability in response to replication stress (1,4). In addition, RAD51 also plays a role in the faithful repair of DSBs. Therefore, the source of self-DNA in the cytosol can originate from defective replication fork processing or defective DSB repair in RAD51-depleted cells. To determine the role of RAD51 in replication fork processing in response to irradiation, we first verified whether RAD51 is recruited to the sites of replication. Most RAD51 foci juxtaposed with EdU foci, representing replication forks, in irradiated but not in mock-treated cells (Figure 4A). Similarly, a major fraction of γ H2AX foci, a surrogate marker for DSBs, juxtaposed with the RAD51 foci upon irradiation (Figure 4A). Thus, these results suggest that RAD51 is localized at the sites of both replication forks and DSBs in response to irradiation. Second, we evaluated replication fork progression, stalling, new origin firing, and stability in RAD51-proficient and -depleted cells after irradiation, using a single-molecule DNA fiber technique (4,25,30). Replication fork lengths (determined using IdU-labeling) were comparable between mock-treated RAD51-proficient and RAD51-depleted cells (5.08 ± 0.06 and 5.01 ± 0.10 μ m in RAD51-proficient and RAD51-depleted cells, respectively; Figure 4B). In contrast, replication fork lengths (labeled with CldU) in irradiated RAD51-depleted cells were significantly shorter than those in irradiated RAD51-proficient cells (4.62 ± 0.04 and 2.89 ± 0.07 μ m in RAD51-proficient and -depleted cells, respectively; $P = 0.006$, Figure 4B). These results indicate that RAD51 is important for replication fork progression in response to irradiation. Subsequently, we verified the efficiency of replication fork restart in irradiated cells. In irradiated RAD51-depleted cells, most DNA fibers (73.42%; $P = 0.02$) had both IdU and CldU tracts, whereas 79.47% fibers contained both IdU and CldU in irradiated RAD51-proficient cells (Figure 4C). These results indicate that a greater proportion of replication forks failed to restart in RAD51-depleted cells in response to irradiation when compared to cells expressing RAD51.

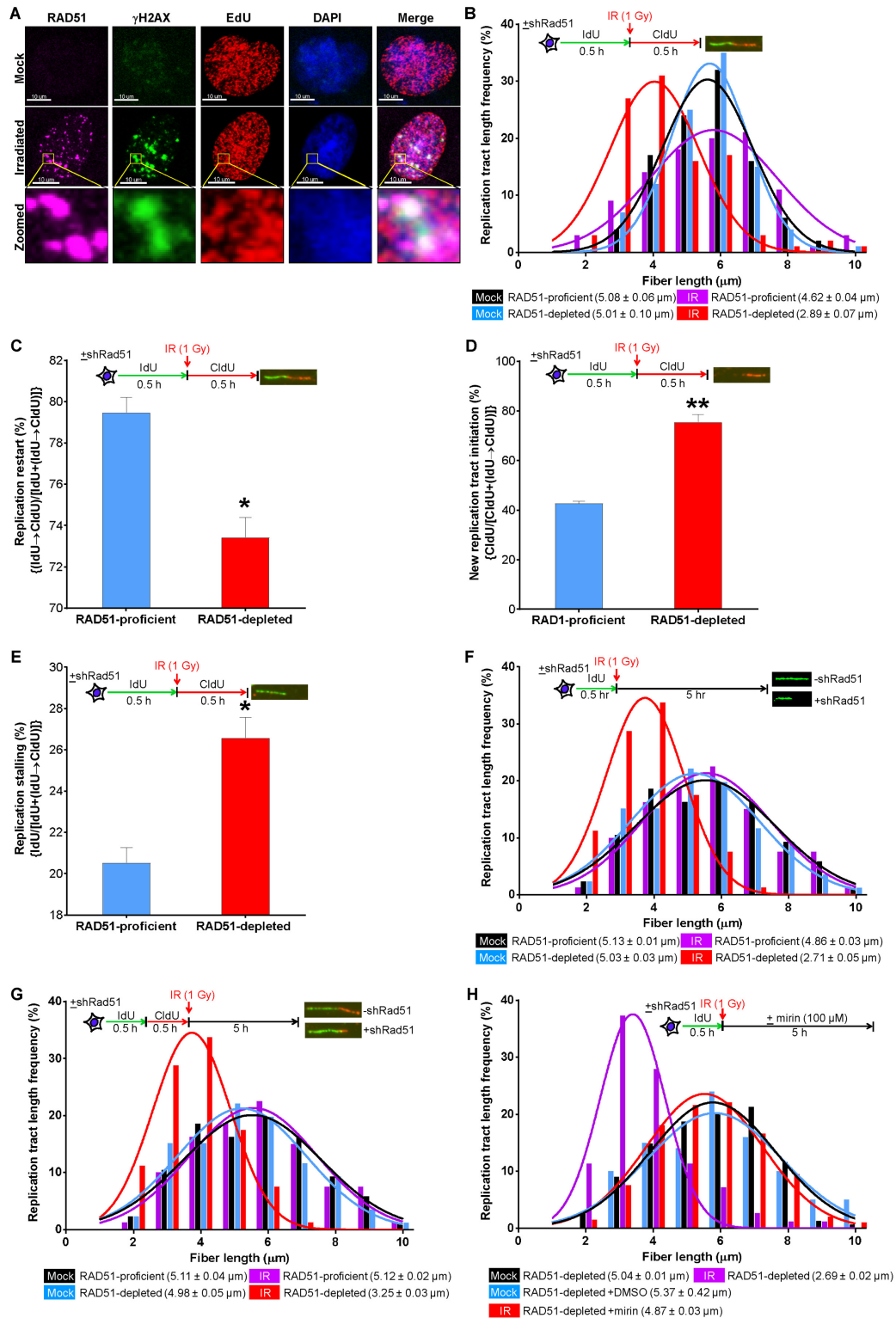


Figure 4. RAD51 blocks the MRE11-mediated degradation of nascent DNA strands upon irradiation. (A) Representative images show the co-localization of RAD51 foci with EdU and γ H2AX foci. HT1080 cells were pulse-labeled with EdU for 30 min and immediately irradiated with 1 Gy, fixed with 4% PFA 4 h after irradiation, and immunostained with anti-RAD51 and anti- γ H2AX antibodies. EdU was detected using the Click-IT reaction. Scale bars are 10 μ m. (B) Replication fork progression is reduced in RAD51-depleted cells in response to irradiation. DNA fiber length distributions in RAD51-proficient and -depleted cells are shown before and after irradiation. Cells were labeled with IdU for 30 min, treated with and without 1 Gy radiation, and labeled with CldU for another 30 min. DNA fibers were immunostained with anti-BrdU (rat and mouse) antibodies. Images were captured using a fluorescence microscope and IdU (before) CldU (after) lengths were measured using Axiovision Software. More than 200 DNA fibers were evaluated in each sample. Each data point is the average of three independent experiments. (C–E) Replication forks stall in RAD51-depleted cells after irradiation. Percentages of replication fork

Next, we investigated new origin firing and replication fork stalling in RAD51-proficient and -depleted cells after irradiation. The number of DNA fibers only containing CldU tracts, representing new origins of replication, was significantly higher in RAD51-depleted cells than in irradiated RAD51-proficient cells (75.50% and 42.66% in RAD51-depleted and -proficient cells, respectively, $P = 0.005$; Figure 4D). In addition, we observed a significantly higher percentage of DNA fibers only containing IdU tracts, which represent stalled forks in irradiated RAD51-depleted cells as compared to irradiated RAD51-proficient cells (26.58% and 20.53% in RAD51-depleted and -proficient cells, respectively, $P = 0.02$; Figure 4E). Taken together, these results suggest that RAD51 is important for the suppression of new origin firing and replication fork stalling after irradiation.

Previous studies have reported that RAD51 is important for the stability of perturbed replication forks in response to replication stress (4,5,43). To verify whether RAD51 stabilizes nascent DNA strands, we labeled the replicating DNA with IdU for 30 min, irradiated it, and measured the lengths of IdU-labeled DNA fibers 5 h after exposure, as previously described (4). Under these conditions, the IdU tract lengths were slightly shorter in mock-treated RAD51-depleted cells relative to mock-treated RAD51-proficient cells; however, this difference is not statistically significant (5.13 ± 0.01 and 5.03 ± 0.03 μm , respectively; Figure 4F). Similarly, the IdU tract lengths were comparable between irradiated and mock-treated RAD51-proficient cells (5.13 ± 0.01 and 4.86 ± 0.03 μm , respectively). In contrast, the IdU tract lengths were significantly shorter in irradiated RAD51-depleted cells than in mock-treated RAD51-proficient cells (2.71 ± 0.05 and 4.86 ± 0.03 μm , respectively, $P = 0.0003$; Figure 4F). This result indicated the degradation of IdU labeled tracts in RAD51-depleted cells. Thus, in addition to playing roles in replication fork progression and efficient restart, RAD51 is also involved in the maintenance of nascent DNA strands in response to irradiation.

Previous studies have confirmed that MRE11 degrades nascent DNA strands in the absence of BRCA2, FA factors, WRN, and RAD51 in response to replication stress (2,4,5,43). Therefore, we hypothesized that MRE11 is the nuclease that degrades nascent DNA strands in the absence of RAD51 during radiation-induced replication

stress. MRE11 has 3'–5' exonuclease and endonuclease activities (44). Therefore, we first examined the direction of nascent DNA strand degradation in RAD51-depleted cells by sequentially labeling the replicating DNA, first with IdU and then with CldU. We observed the shortening of recently replicated DNA (i.e. CldU-labeled DNA) in irradiated RAD51-depleted cells (5.12 ± 0.02 and 3.25 ± 0.03 μm , RAD51-proficient and -depleted cells, respectively), suggesting that the nascent DNA strands were degraded in a 3' to a 5' direction (Figure 4G). Thus, the degradation of nascent DNA strands in RAD51 down-regulated cells is mediated by the exonuclease activity of MRE11. To further confirm these results, we inhibited the exonuclease activity of MRE11 with mirin (45) and examined nascent DNA strand lengths. The IdU tract lengths were not shortened in irradiated cells pre-treated with mirin (Figure 4H). The DNA fiber lengths in irradiation+mirin-treated RAD51-depleted cells were comparable to those of mock+mirin-treated RAD51-depleted cells (4.87 ± 0.03 and 5.37 ± 0.42 μm , respectively; Figure 4H). Thus, these degraded nascent DNA strands accumulate in the cytosol, triggering an innate immune response in RAD51-depleted cells after irradiation.

Blocking of the MRE11-mediated degradation of newly replicated genome attenuates cytosolic self-DNA accumulation in RAD51-depleted cells

To confirm that the MRE11-processed newly replicated genome accumulates in the cytosol of RAD51-depleted cells, we pre-treated cells with mirin followed by irradiation. Subsequently, we quantified the amount of ssDNA and dsDNA in the cytosolic fraction. We observed a significant reduction in the cytosolic ssDNA amount in mirin+radiation treated RAD51-depleted cells as compared to irradiated RAD51-depleted cells 8 h post-irradiation (19.91 ± 3.05 and 14.36 ± 0.65 $\text{pg}/\mu\text{g}$ protein in radiation alone and radiation+mirin treated RAD51-depleted cells, respectively; $P < 0.0002$; Figure 5A). Similarly, the amount of cytosolic dsDNA was also significantly reduced in mirin+radiation treated RAD51-depleted cells as compared to irradiated RAD51-depleted cells (9.35 ± 0.68 and 5.51 ± 0.43 $\text{pg}/\mu\text{g}$ protein in radiation alone and radiation+mirin treated RAD51-depleted cells, respectively; $P < 0.0002$; Figure 5B). Furthermore, the amount of cytosolic ssDNA and

restarts in irradiated RAD51-proficient and -depleted cells relative to mock-treated cells were evaluated using the $\{(\text{IdU} \rightarrow \text{CldU})/[\text{IdU} + (\text{IdU} \rightarrow \text{CldU})]\}$ formula (C). Percentage changes in new origin firing in irradiated RAD51-proficient and -depleted cells as compared to mock-treated cells were calculated using the $\{\text{CldU}/[\text{CldU} + (\text{IdU} \rightarrow \text{CldU})]\}$ formula (D). Percentage changes in replication forks stalling in RAD51-proficient and -depleted cells as compared to mock-irradiated cells were evaluated using the $\{\text{IdU}/[\text{IdU} + (\text{IdU} \rightarrow \text{CldU})]\}$ formula (E). More than 200 DNA fibers were evaluated in each sample. Each data point is the average of two independent experiments. Error bars represent the STDEV; * $P < 0.05$; ** $P < 0.01$. (F) Nascent DNA strands were shortened in RAD51-depleted cells. Replicating DNA in RAD51-proficient and -depleted cells was labeled with IdU for 30 min and irradiated with 1 Gy. DNA fibers were immunostained with anti-BrdU (mouse) antibodies. DNA fiber images were captured using a fluorescence microscope, and IdU tract lengths were measured using the Axiovision Software. The frequency distributions of the lengths of more than 100 DNA fibers were calculated from three independent experiments in each group. (G) Newly replicated DNA was shortened in the absence of RAD51. Shortening of newly synthesized DNA fiber length distributions in RAD51-proficient and -depleted cells 5 h after irradiation. Cells were labeled with IdU for 30 min and then with CldU for another 30 min. Subsequently, cells were irradiated with 1 Gy. Five hours after irradiation, DNA fibers were immunostained with anti-BrdU (rat and mouse) antibodies, images were captured using a fluorescence microscope, and CldU tract lengths were measured using the Axiovision Software. More than 200 DNA fibers were evaluated in each sample. Each data point is the average of three independent experiments. (H) RAD51 blocks the MRE11-mediated degradation of nascent DNA strands in response to irradiation. RAD51-proficient and -depleted cells were labeled with IdU for 30 min. Cells were pre-treated with or without 100 μM of the MRE11 exonuclease inhibitor (mirin), irradiated with 1 Gy. Five hours after irradiation, DNA fibers were immunostained with anti-BrdU (mouse). Images were captured using a fluorescence microscope and IdU tract lengths were measured using the Axiovision Software. More than 100 DNA fibers were evaluated in each sample. Each data point is the average of two independent experiments.

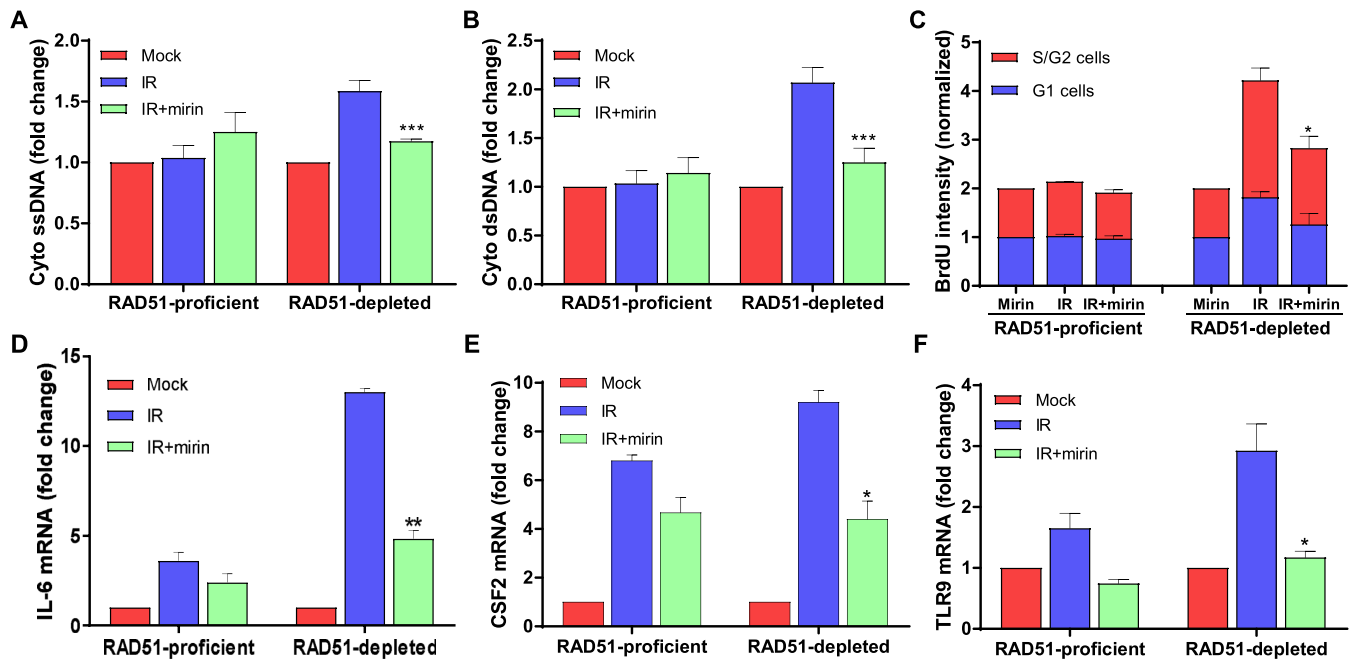


Figure 5. Inhibition of MRE11 exonuclease activity blocks the expression of innate immune response genes in RAD51-depleted cells. (A and B) The quantification of ssDNA and dsDNA DNA in the cytosol. RAD51-proficient and -depleted cells were pre-treated with mirin (25 μ M), irradiated with 2 Gy and harvested 8 h after irradiation. Subsequently, cells were subjected to sub-cellular fractionation and the amount of cytosolic ssDNA (A) and dsDNA (B) were quantified using OliGreen and PicoGreen Quant-iT reagents, respectively. The bars represent the changes in the cytoplasmic DNA concentration relative to respective mock-treated samples. Error bars represent STDEV from four independent experiments; *** $P < 0.001$. (C) The quantification of the cytoplasmic BrdU signal normalized to mock-treated RAD51-proficient samples. RAD51-proficient and -depleted HT1080-FUCCI cells were labeled with BrdU for 18–20 h, pre-treated with mirin (25 μ M), irradiated with 2 Gy and fixed with ice cold 80% methanol in PBS 8 h after irradiation. Cells were immunostained with an anti-BrdU antibody under non-denaturing conditions. Subsequently, cells were imaged using a LSM510 confocal microscope and the BrdU signal in the cytoplasm of G1 and S/G2 phase cells was quantified using the ZEN 2009 (version 6.0.0303) Software (Carl Zeiss, Jena, Germany). Bars represent mean cytoplasmic BrdU fluorescence intensity per cell relative to respective mirin-treated control G1 and S/G2 cells. More than 150 cells were used for quantification in each condition. Error bars represent the STDEV from two-four independent experiments; * $P < 0.05$. (D and F) Down-regulation of IL-6, CSF2, and TLR9 expression in cells pre-treated with the MRE11 exonuclease inhibitor. RAD51-proficient and -depleted cells were pre-treated with mirin (25 μ M) and irradiated with 1 Gy; total RNA was prepared 8 h after irradiation. mRNAs were converted into cDNA and the levels of IL-6 (D), CSF2 (E) and TLR9 (F) mRNA were quantified by qRT-PCR. Error bars represent the SEM from three-four independent experiments; * $P < 0.05$; ** $P < 0.01$.

dsDNA in radiation+mirin treated RAD51-depleted cells was slightly higher than the mock-radiation+mirin treated RAD51-depleted cells. Thus, the excessive nuclease activity of MRE11 on the newly replicated genome in the absence of RAD51 contributes to the majority of cytosolic self-DNA accumulation upon replication stress induced by irradiation.

In addition to the pharmacological inhibition of MRE11 in RAD51-depleted HT1080 cells, we confirmed the contribution of MRE11-mediated degradation of nascent DNA strands in the accumulation of cytosolic DNA in the absence of RAD51 by both pharmacological (SAHA) and genetic (shRNA) down-regulation of RAD51 expression in MRE11-deficient ATLD cells (4). We found that neither the genetic (shRad51) nor the pharmacological (SAHA)-mediated down-regulation of RAD51 significantly increased cytosolic-DNA in the absence of MRE11 upon irradiation (Supplementary Figure S2). These results indicate that the RAD51-mediated blocking of MRE11-dependent degradation of nascent DNA suppresses the innate immune response upon irradiation.

To further validate the influence of MRE11 on cytosolic self-DNA accumulation, we measured cytoplasmic

BrdU levels after inhibiting MRE11 exonuclease activity. The cytoplasmic BrdU fluorescent intensity was unaltered in mirin+radiation treated RAD51-proficient cells as compared to irradiated RAD51-proficient cells (5.24 ± 0.02 and 4.68 ± 0.11 MFI per cell for radiation alone and mirin+radiation samples, respectively; Figure 5C). On the other hand, mirin+irradiation treated RAD51-depleted cells exhibited significantly reduced levels of cytoplasmic BrdU signal (7.46 ± 0.57 MFI per cell; $P < 0.0001$) as compared to irradiated RAD51-depleted cells (10.92 ± 0.08 MFI per cell). Cell cycle specific analysis of BrdU intensity in irradiated RAD51-depleted cells further revealed compared to G1 cells (9.57 ± 0.09 and 7.0 ± 1.38 MFI per G1 cell for irradiation alone and mirin+irradiation samples, respectively) mirin-treated RAD51-depleted S/G2 cells showed reduced cytoplasmic BrdU levels relative to control treated irradiated S/G2 cells (12.26 ± 0.06 and 7.9 ± 0.23 MFI per S/G2 cell for radiation alone and mirin+irradiation samples, respectively, $P < 0.05$). Collectively, MRE11-mediated degradation of the newly replicated genome is partially responsible for the increased amount of self-DNA in the cytosol of RAD51-depleted cells.

However, it is still unclear whether the attenuation of cytosolic self-DNA by the targeted inhibition of MRE11 exonuclease activity can actually limit the expression of innate immune response genes. Hence, we measured expression levels of IL-6, CSF2, and TLR9 by qRT-PCR. These three genes showed maximum upregulation in irradiated RAD51-depleted cells, but were significantly reduced in mirin+radiation-treated RAD51-depleted cells as compared to radiation only RAD51-depleted cells ($P < 0.02-0.002$; Figure 5D-F). Taken together, our data suggest that a significant proportion of cytoplasmic self-DNA comes from the MRE11-mediated excessive processing of nascent DNA strands, contributing to the initiation of innate immunity in RAD51-depleted cells in response to irradiation.

DSBs are difficult to repair in RAD51-depleted S/G2 cells

Although the amount of self-DNA is decreased in mirin-treated RAD51-depleted cells, the mirin treatment did not reduce cytosolic self-DNA to the basal level. This observation suggests that apart from processed nascent DNA strand, other cellular sources can contribute to the self-DNA accumulation in the cytoplasm. Furthermore, evidence indicates that in the absence of ATM, unrepaired DNA lesions contribute to the increased amount of cytosolic self-DNA, activating a STING-mediated innate immune response (14). Therefore, we hypothesized that a lack of RAD51 may lead to defective DSBs repair. Because the RAD51-dependent HR-mediated DSB repair pathway is involved in S/G2 phase of the cell cycle, the unrepaired DSBs may persist in S/G2 phase of RAD51-depleted cells. To verify this, we enumerated γ H2AX foci dissolution kinetics in G1 and S/G2 phases of HT1080-FUCCI cells (30), using an algorithm developed in MatLab. We detected γ H2AX foci in G1 and S/G2 RAD51-proficient and RAD51-depleted cells at different time points after irradiation (Figure 6A-B and Supplementary Table S2). The levels of γ H2AX foci were comparable between G1-phase RAD51-proficient and G1-phase RAD51-depleted cells 24 h after irradiation (3.56 and 4.54% in RAD51-proficient and -depleted cells, respectively, Figure 6C and Supplementary Table S2). In contrast, the percentages of persistent γ H2AX foci were significantly elevated in RAD51-depleted S/G2 cells as compared to RAD51-proficient cells 24 h after irradiation (62.96 + 5.17% and 12.68%, respectively, $P < 0.001$; Figure 6C and Supplementary Table S2). Thus, these results suggest that RAD51-depleted S/G2 cells cannot fully repair the DSBs induced by irradiation. Also, similarly to ATM, defective DSB repair in RAD51-depleted cells may partially contribute to the elevated levels of cytosolic self-DNA.

To further investigate the consequences of defects in DNA replication and DSB repair in RAD51-depleted cells, we evaluated their cellular phenotype. First, we examined cellular survival by colony formation assay. Similar to a previous report (20), RAD51-depleted cells were more sensitive to irradiation than RAD51-proficient cells (Figure 6D). Additionally, pre-treatment of RAD51-depleted cells with mirin partially rescued irradiation-induced cell survival (Figure 6D). These results imply that RAD51 together with the exonuclease activity of MRE11 influences cellu-

lar survival upon irradiation. Furthermore, we noticed that inhibition of STAT3 significantly decreased the survival of RAD51-depleted cells relative to RAD51-proficient cells (Supplementary Figure S3), suggesting a role for STAT3 in enhancing the sensitivity of RAD51-depleted cells to ionizing radiation.

Second, we investigated chromosome instability. Conventional chromosome analysis of metaphase spreads revealed that the levels of chromosomal aberrations per mitotic cells were significantly elevated in irradiated RAD51-depleted cells as compared to the number of aberrations in irradiated RAD51-proficient cells (Figure 6E). The average number of aberrations per irradiated RAD51-depleted mitotic cells was 5.18 ± 0.42 ($P < 0.007$), as compared to only 1.56 ± 0.04 in irradiated RAD51-proficient mitotic cells. The number of chromatid-type aberrations was significantly elevated in irradiated RAD51-depleted mitotic cells (2.94 ± 0.32 , $P = 0.008$) as compared to irradiated RAD51-proficient mitotic cells (0.38 ± 0.04 ; Figure 6E).

MRE11-mediated degradation of a newly replicated genome in the absence of RAD51 contributes to self-DNA accumulation in the cytosol. To further delineate the role of MRE11-exonuclease activity in chromosome stability maintenance, we inhibited the exonuclease activity of MRE11 in irradiated cells and examined chromosome aberrations (Figure 6E). We noticed that the suppression of exonuclease activity of MRE11 resulted in a significant reduction of gross-chromosomal aberrations in irradiated RAD51-depleted mitotic cells (2.11 ± 0.042 ; $P = 0.01$) as compared to irradiated RAD51-depleted mitotic cells (Figure 6E). Overall, these results demonstrate the role of RAD51 in the suppression of chromosomal instability.

DISCUSSION

We identified the role of RAD51 in innate immune signaling in response to DNA damage and replication stress. RAD51 is recruited to the sites of DSBs, facilitating their repair in S/G2 phase cells. In addition, RAD51 is also recruited to the perturbed replication forks, preventing MRE11-mediated excessive processing of newly replicated genomes. Replication fork degradation combined with defects in DSB repair leads to the accumulation of self-DNA in the cytosol, resulting in the initiation of a STING-mediated innate immune response in cells lacking RAD51. Thus, the coordinated activities of RAD51 in DSB repair, replication fork maintenance, and innate immune response signaling provide new insights into carcinogenesis associated with defective RAD51 functions.

We found that defects in RAD51 impact innate immune response signaling upon DNA damage and replication stress. This result was unexpected because there is no evidence of the RAD51 involvement in innate immunity upon irradiation. However, this phenomenon is not limited to RAD51 but has also been reported in other cell types defective in DNA repair and replication factors. For example, the DNA damage sensor MRE11, plays important roles in the recognition of dsDNA and the initiation of STING-dependent immune response signaling, though this is not the case for its nuclease activity (15). The loss of ATM culminates in enhanced constitutive production of type I inter-

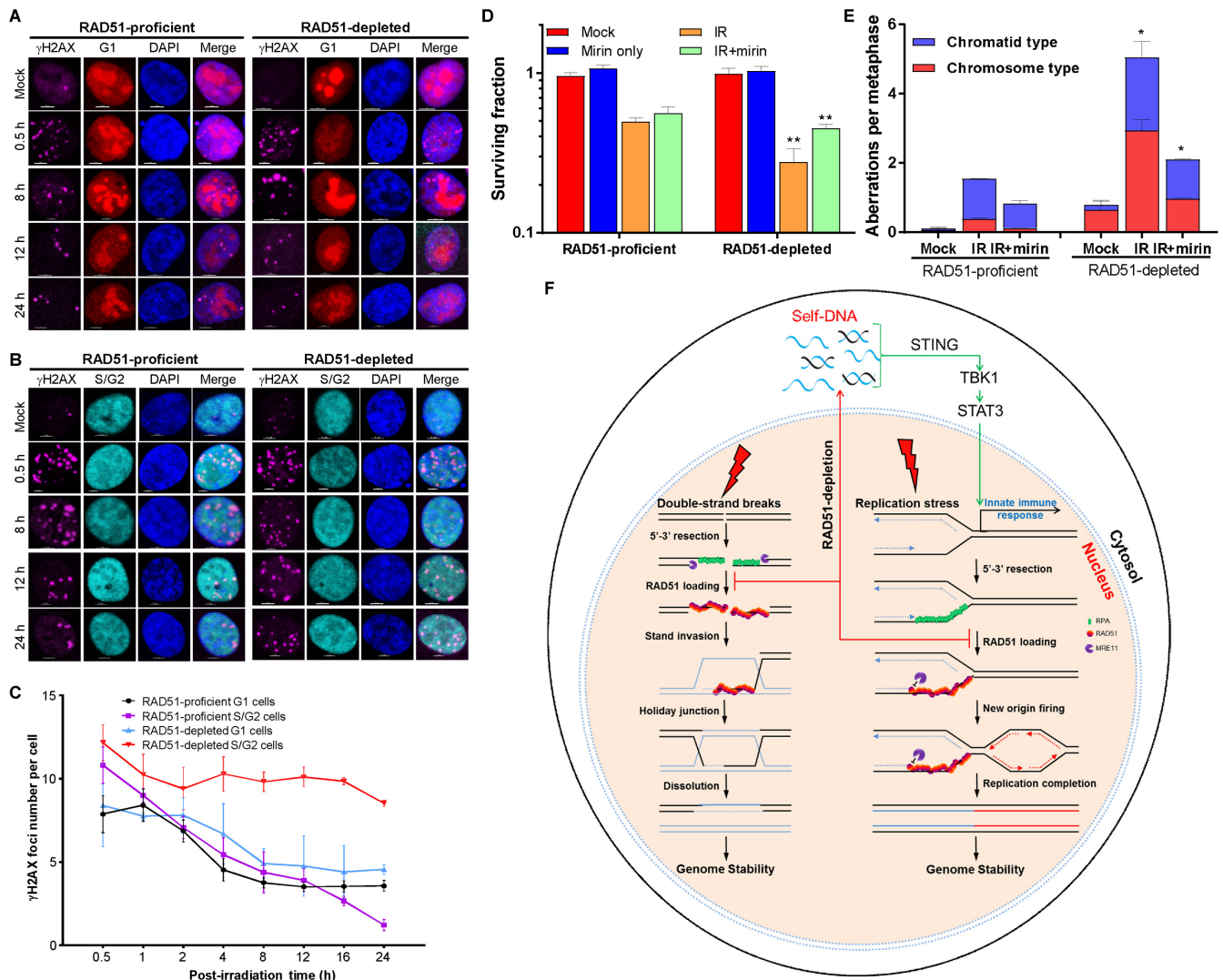


Figure 6. RAD51 is critical for DSB repair in S/G2 cells and chromosome stability maintenance. (A–C) DSBs persist in RAD51-depleted S/G2 cells: Representative images show appearance and disappearance of γ H2AX foci in G1 (A) and S/G2 (B) cells. Cell cycle-dependent γ H2AX foci dissolution kinetics in RAD51-proficient and -depleted HT1080 cells stably expressing two different cell cycle markers, mCherry (G1) and AmCyan (S/G2) (C). Cells were irradiated with 1 Gy and immunostained with anti- γ H2AX at the indicated times after irradiation. Cells were imaged using a confocal microscope and γ H2AX foci in 100–120 red and Cyan fluorescent cells representing G1 and S/G2 phases, respectively were counted using the Matlab software (Mathworks, MA). Error bars represent the STDEV from three-four independent experiments. Scale bars are 5 μ m. (D) RAD51-depleted cells are sensitive to irradiation. RAD51-proficient and -depleted cells plated in six well plates were exposed to 0.5 Gy of radiation with or without mirin treatment and cell survival was analyzed by a colony formation assay. Colonies were fixed and counted 8–10 days after irradiation. The relative survival efficiencies were plotted. The error bars represent the STDEV calculated from triplicate wells; ** $P < 0.01$. (E) RAD51 suppresses chromosome instability upon irradiation. Number of chromatid and chromosome-type aberrations in mock- and -irradiated RAD51-proficient and -depleted cells pre-treated with and without mirin. Exponentially growing cells were either mock-treated or irradiated with 1 Gy, and the metaphase chromosomes spreads were prepared 16 h after treatment. Chromosomal aberrations in > 100 metaphase spreads were scored from two to four independent experiments in each group. Error bars represent the STDEV calculated from two-four independent experiments; * $P < 0.05$. (F) RAD51 interconnects between replication fork processing, DSB repair, and innate immune responses. The model depicts the mechanism of innate immunity initiation in RAD51-depleted cells due to defective replication fork processing and DSB repair.

ferons, elevated expression of different pattern recognition receptors, and their downstream signaling partners, which together contribute to priming the innate immune system (14). In addition, the DNA structure-specific endonuclease MUS81 that cleaves DNA structures at stalled replication forks also mediates the STING-dependent activation of innate immune signaling (16). FA proteins were recently identified as key players in immunity (17). Furthermore, RPA2 and RAD51 prevent the release of short nuclear DNA frag-

ments into the cytosol by binding to these DNA fragments thereby preventing immune response signaling (18). Thus, DNA repair and replication factors participate in immune signaling outside their known DNA repair and replication functions.

Our results suggest two potential mechanisms by which RAD51-deficiency may lead to cytosolic self-DNA accumulation: i. faulty replication fork maintenance and ii. defective DSB repair. We found that the excessive nuclease ac-

tivity of MRE11 on the newly replicated genome in RAD51 down-regulated cells is a major source of cytosolic-DNA in response to replication stress induced by irradiation. The excessive processing of newly replicated genome by MRE11 in RAD51-depleted cells is not unique to radiation-induced replication stress, but has also been observed in response to agents such as hydroxyurea, camptothecin and gemcitabine (4,5,43). Additionally, RAD51 is the key factor involved in HR-mediated DSB repair in S/G2 cells and its down-regulation results in DSB defects in S/G2 phase cells. These findings suggest that defects associated with DSB repair could be an additional source of cytosolic self-DNA accumulation in RAD51-depleted cells, similarly to the accumulation of cytosolic self-DNA in ATM defective cells (14). However, more studies are needed to identify the mechanism by which irreparable DSBs contribute to the cytosolic self-DNA accumulation in RAD51-depleted cells.

The dysregulation of RAD51 levels and defects associated with RAD51-interacting proteins are known to cause cancer. Carcinogenesis is a multistage process resulting from a cumulative malfunctioning of DNA replication, DSB repair, and immune signaling. Defective DSB repair and replication fork processing may cause genetic and epigenetic mutations, initiating cell transformation and cancer. Our classic chromosome analysis revealed that the levels of chromosomal aberrations were significantly elevated in irradiated RAD51-depleted cells as compared to RAD51-proficient cells. Similarly to BRCA2 defective cells after replication fork stalling (5), the inhibition of the MRE11 exonuclease activity leads to a reduction in the number of chromosomal aberrations in irradiated RAD51-depleted cells, suggesting that maintenance of nascent DNA strands is critical for the prevention of chromosomal instability. Although the irradiation of RAD51-depleted cells compromises cell survival, some cells with chromosomal aberrations can still enter mitosis. Every subsequent round of replication is expected to increase the overall mutation level in surviving cells; a damaged genome can provide an opportunity for genomic rearrangement and can increase genomic instability, leading to genetic changes required to initiate cell transformation and cancer. Activation of the immune system can promote tumor progression by inducing tissue remodeling, supporting angiogenesis, and providing growth factors to the tumor microenvironment that sustains proliferative signaling. This activation also stimulates survival factors that limit cell death, proangiogenic factors, extracellular matrix-modifying enzymes that facilitate angiogenesis, invasion, and metastasis, and triggers inductive signals that lead to the activation of epithelial-mesenchymal transition (46). Our study suggests that RAD51 may function as a tumor suppressor by facilitating faithful DSB repair and replication forks processing, preventing immune signaling. Additional *in vivo* experiments are required to study the contribution of RAD51 in tumor progression upon replication stress and DNA damage.

We propose a model that represents the interplay between RAD51 and immune signaling in response to DNA damage and replication stress (Figure 6F). RAD51 is recruited to the sites of perturbed replication forks and DSBs, resulting in the blockage of the excess exonuclease activity of MRE11 on the newly replicated genome and DSB repair. Conse-

quently, this activity limits the accumulation of self-DNA in the cytosol and prevents the initiation of STING-mediated innate immune response signaling. Thus, RAD51 plays a direct role in DNA replication and DSBs repair, and is indirectly involved in immune signaling.

SUPPLEMENTARY DATA

Supplementary Data are available at NAR Online.

ACKNOWLEDGEMENTS

We thank Dr Shiao-Yih Lin (MD Anderson Cancer Center) for providing the MCF10A cell line stably expressing scrambled and Rad51 shRNA. We thank Dr Damiana Chiavolini for the critical reading of this manuscript. We thank, Drs Peter Guida, Adam Rusek, Mike Sivertz, Chiara La Tessa, Eiichiro Mori and other members of the NASA Space Radiation Laboratory, NY for their help with heavy-ion radiation.

Authors' contributions: S.B, K.S, S.A, S.M and A.A. designed and performed experiments, analyzed data, and performed critical experiments during the revision. F.S. performed DNA fiber and part of chromosome analyses. R.M, P.R. and I.D. performed microarray data mining. S.G. and E.W. contributed to reagents. A.A. conceived the idea and designed experiments. S.B. and A.A. wrote the manuscript.

FUNDING

National Aeronautics and Space Administration [NNX13AD57G and NNX15AE06G]; Cancer Prevention and Research Institute of Texas [RP160520]; National Institute of Health [R01AG053341] to A.A. Funding for open access charge: National Aeronautics and Space Administration.

Conflict of interest statement. None declared.

REFERENCES

- Petermann,E., Orta,M.L., Issaeva,N., Schultz,N. and Helleday,T. (2010) Hydroxyurea-stalled replication forks become progressively inactivated and require two different RAD51-mediated pathways for restart and repair. *Mol. Cell*, **37**, 492–502.
- Hashimoto,Y., Ray Chaudhuri,A., Lopes,M. and Costanzo,V. (2010) Rad51 protects nascent DNA from Mre11-dependent degradation and promotes continuous DNA synthesis. *Nat. Struct. Mol. Biol.*, **17**, 1305–1311.
- Krishna,S., Wagener,B.M., Liu,H.P., Lo,Y.C., Sterk,R., Petrini,J.H. and Nickoloff,J.A. (2007) Mre11 and Ku regulation of double-strand break repair by gene conversion and break-induced replication. *DNA Repair (Amst.)*, **6**, 797–808.
- Su,F., Mukherjee,S., Yang,Y., Mori,E., Bhattacharya,S., Kobayashi,J., Yannone,S.M., Chen,D.J. and Asaithamby,A. (2014) Nonenzymatic role for WRN in preserving nascent DNA strands after replication stress. *Cell Rep.*, **9**, 1387–401.
- Schlacher,K., Wu,H. and Jasin,M. (2012) A distinct replication fork protection pathway connects Fanconi anemia tumor suppressors to RAD51-BRCA1/2. *Cancer Cell*, **22**, 106–116.
- Lundin,C., Schultz,N., Arnaudeau,C., Mohindra,A., Hansen,L.T. and Helleday,T. (2003) RAD51 is involved in repair of damage associated with DNA replication in mammalian cells. *J. Mol. Biol.*, **328**, 521–535.
- Tsuzuki,T., Fujii,Y., Sakumi,K., Tominaga,Y., Nakao,K., Sekiguchi,M., Matsushiro,A., Yoshimura,Y. and Morita,T. (1996) Targeted disruption of the Rad51 gene leads to lethality in embryonic mice. *Proc. Natl. Acad. Sci. U.S.A.*, **93**, 6236–6240.

8. Silva, M.C., Morrical, M.D., Bryan, K.E., Averill, A.M., Dragon, J., Bond, J.P. and Morrical, S.W. (2016) RAD51 variant proteins from human lung and kidney tumors exhibit DNA strand exchange defects. *DNA Repair (Amst.)*, **42**, 44–55.
9. Prakash, R., Zhang, Y., Feng, W. and Jasin, M. (2015) Homologous recombination and human health: the roles of BRCA1, BRCA2, and associated proteins. *Cold Spring Harb. Perspect. Biol.*, **7**, a016600.
10. Schild, D. and Wiese, C. (2010) Overexpression of RAD51 suppresses recombination defects: a possible mechanism to reverse genomic instability. *Nucleic Acids Res.*, **38**, 1061–1070.
11. Yoshikawa, K., Ogawa, T., Baer, R., Hemmi, H., Honda, K., Yamauchi, A., Inamoto, T., Ko, K., Yazumi, S., Motoda, H. *et al.* (2000) Abnormal expression of BRCA1 and BRCA1-interactive DNA-repair proteins in breast carcinomas. *Int. J. Cancer*, **88**, 28–36.
12. Nowarski, R., Gagliani, N., Huber, S. and Flavell, R.A. (2013) Innate immune cells in inflammation and cancer. *Cancer Immunol. Res.*, **1**, 77–84.
13. Goldszmid, R.S. and Trinchieri, G. (2012) The price of immunity. *Nat. Immunol.*, **13**, 932–938.
14. Hartlova, A., Erttmann, S.F., Raffi, F.A., Schmalz, A.M., Resch, U., Anugula, S., Lienenklaus, S., Nilsson, L.M., Kröger, A., Nilsson, J.A. *et al.* (2015) DNA damage primes the type I interferon system via the cytosolic DNA sensor STING to promote anti-microbial innate immunity. *Immunity*, **42**, 332–343.
15. Kondo, T., Kobayashi, J., Saitoh, T., Maruyama, K., Ishii, K.J., Barber, G.N., Komatsu, K., Akira, S., Kawai, T. *et al.* (2013) DNA damage sensor MRE11 recognizes cytosolic double-stranded DNA and induces type I interferon by regulating STING trafficking. *Proc. Natl. Acad. Sci. U.S.A.*, **110**, 2969–2974.
16. Ho, S.S., Zhang, W.Y., Tan, N.Y., Khatoo, M., Suter, M.A., Tripathi, S., Cheung, F.S., Lim, W.K., Tan, P.H., Ngeow, J. *et al.* (2016) The DNA structure-specific endonuclease MUS81 mediates DNA sensor STING-dependent host rejection of prostate cancer cells. *Immunity*, **44**, 1177–1189.
17. Sumpter, R. Jr, Sirasanagandla, S., Fernández, Á.F., Wei, Y., Dong, X., Franco, L., Zou, Z., Marchal, C., Lee, M.Y., Clapp, D.W. *et al.* (2016) Fanconi anemia proteins function in mitophagy and immunity. *Cell*, **165**, 867–881.
18. Wolf, C., Rapp, A., Berndt, N., Staroske, W., Schuster, M., Dobrick-Mattheuer, M., Kretschmer, S., König, N., Kurth, T., Wiczorek, D. *et al.* (2016) RPA and Rad51 constitute a cell intrinsic mechanism to protect the cytosol from self DNA. *Nat. Commun.*, **7**, 11752.
19. Asaithamby, A. and Chen, D.J. (2009) Cellular responses to DNA double-strand breaks after low-dose gamma-irradiation. *Nucleic Acids Res.*, **37**, 3912–3923.
20. Zafar, F., Seidler, S.B., Kronenberg, A., Schild, D. and Wiese, C. (2010) Homologous recombination contributes to the repair of DNA double-strand breaks induced by high-energy iron ions. *Radiat. Res.*, **173**, 27–39.
21. Peng, G., Chun-Jen Lin, C., Mo, W., Dai, H., Park, Y.Y., Kim, S.M., Peng, Y., Mo, Q., Siwko, S., Hu, R. *et al.* (2014) Genome-wide transcriptome profiling of homologous recombination DNA repair. *Nat. Commun.*, **5**, 3361.
22. Takeshima, T., Pop, L.M., Laine, A., Iyengar, P., Vitetta, E.S. and Hannan, R. (2016) Key role for neutrophils in radiation-induced antitumor immune responses: potentiation with G-CSF. *Proc. Natl. Acad. Sci. U.S.A.*, **113**, 11300–11305.
23. Asaithamby, A., Hu, B., Delgado, O., Ding, L.H., Story, M.D., Minna, J.D., Shay, J.W. and Chen, D.J. (2011) Irreparable complex DNA double-strand breaks induce chromosome breakage in organotypic three-dimensional human lung epithelial cell culture. *Nucleic Acids Res.*, **39**, 5474–5488.
24. Puente, B.N., Kimura, W., Muralidhar, S.A., Moon, J., Amatruda, J.F., Phelps, K.L., Grinsfelder, D., Rothermel, B.A., Chen, R., Garcia, J.A. *et al.* (2014) The oxygen-rich postnatal environment induces cardiomyocyte cell-cycle arrest through DNA damage response. *Cell*, **157**, 565–579.
25. Su, F., Bhattacharya, S., Abdisalaam, S., Mukherjee, S., Yajima, H., Yang, Y., Mishra, R., Srinivasan, K., Ghose, S., Chen, D.J. *et al.* (2016) Replication stress induced site-specific phosphorylation targets WRN to the ubiquitin-proteasome pathway. *Oncotarget*, **7**, 46–65.
26. Rocke, D.M. and Durbin, B. (2001) A model for measurement error for gene expression arrays. *J. Comput. Biol.*, **8**, 557–569.
27. Dozmorov, I. and Centola, M. (2003) An associative analysis of gene expression array data. *Bioinformatics*, **19**, 204–211.
28. Dozmorov, I. and Lefkovits, I. (2009) Internal standard-based analysis of microarray data. Part 1: analysis of differential gene expressions. *Nucleic Acids Res.*, **37**, 6323–6339.
29. Dozmorov, M.G., Guthridge, J.M., Hurst, R.E. and Dozmorov, I.M. (2010) A comprehensive and universal method for assessing the performance of differential gene expression analyses. *PLoS One*, **5**, e12657.
30. Zhu, J., Su, F., Mukherjee, S., Mori, E., Hu, B. and Asaithamby, A. (2015) FANCD2 influences replication fork processes and genome stability in response to clustered DSBs. *Cell Cycle*, **14**, 1809–1822.
31. Asaithamby, A., Hu, B. and Chen, D.J. (2011) Unrepaired clustered DNA lesions induce chromosome breakage in human cells. *Proc. Natl. Acad. Sci. U.S.A.*, **108**, 8293–8298.
32. Deng, L., Liang, H., Xu, M., Yang, X., Burnette, B., Arina, A., Li, X.D., Mauceri, H., Beckett, M., Darga, T. *et al.* (2014) STING-dependent cytosolic DNA sensing promotes radiation-induced type I interferon-dependent antitumor immunity in immunogenic tumors. *Immunity*, **41**, 843–852.
33. Utz, P.J. and Anderson, P. (2000) Life and death decisions: regulation of apoptosis by proteolysis of signaling molecules. *Cell Death Differ.*, **7**, 589–602.
34. Boulares, A.H., Yakovlev, A.G., Ivanova, V., Stoica, B.A., Wang, G., Iyer, S. and Smulson, M. (1999) Role of poly(ADP-ribose) polymerase (PARP) cleavage in apoptosis. Caspase 3-resistant PARP mutant increases rates of apoptosis in transfected cells. *J. Biol. Chem.*, **274**, 22932–22940.
35. Chen, X., Wong, P., Radany, E.H., Stark, J.M., Lallier, C. and Wong, J.Y. (2012) Suberoylanilide hydroxamic acid as a radiosensitizer through modulation of RAD51 protein and inhibition of homology-directed repair in multiple myeloma. *Mol. Cancer Res.*, **10**, 1052–1064.
36. Liu, Y.P., Zeng, L., Tian, A., Bomkamp, A., Rivera, D., Gutman, D., Barber, G.N., Olson, J.K. and Smith, J.A. (2012) Endoplasmic reticulum stress regulates the innate immunity critical transcription factor IRF3. *J. Immunol.*, **189**, 4630–4639.
37. Tanaka, Y. and Chen, Z.J. (2012) STING specifies IRF3 phosphorylation by TBK1 in the cytosolic DNA signaling pathway. *Sci. Signal.*, **5**, ra20.
38. Abe, T. and Barber, G.N. (2014) Cytosolic-DNA-mediated, STING-dependent proinflammatory gene induction necessitates canonical NF- κ B activation through TBK1. *J. Virol.*, **88**, 5328–5341.
39. Liu, S., Cai, X., Wu, J., Cong, Q., Chen, X., Li, T., Du, F., Ren, J., Wu, Y.T., Grishin, N.V. *et al.* (2015) Phosphorylation of innate immune adaptor proteins MAVS, STING, and TRIF induces IRF3 activation. *Science*, **347**, aaa2630.
40. Ahn, J., Xia, T., Konno, H., Konno, K., Ruiz, P. and Barber, G.N. (2014) Inflammation-driven carcinogenesis is mediated through STING. *Nat. Commun.*, **5**, 5166.
41. Yang, Y.G., Lindahl, T. and Barnes, D.E. (2007) Trex1 exonuclease degrades ssDNA to prevent chronic checkpoint activation and autoimmune disease. *Cell*, **131**, 873–886.
42. Stetson, D.B., Ko, J.S., Heidmann, T. and Medzhitov, R. (2008) Trex1 prevents cell-intrinsic initiation of autoimmunity. *Cell*, **134**, 587–598.
43. Schlacher, K., Christ, N., Siaud, N., Egashira, A., Wu, H. and Jasin, M. (2011) Double-strand break repair-independent role for BRCA2 in blocking stalled replication fork degradation by MRE11. *Cell*, **145**, 529–542.
44. Shibata, A., Moiani, D., Arvai, A.S., Perry, J., Harding, S.M., Genois, M.M., Maity, R., van Rossum-Fikkert, S., Kertokallio, A., Romoli, F. *et al.* (2014) DNA double-strand break repair pathway choice is directed by distinct MRE11 nuclease activities. *Mol. Cell*, **53**, 7–18.
45. Dupre, A., Boyer-Chatenet, L., Sattler, R.M., Modi, A.P., Lee, J.H., Nicolette, M.L., Kopelovich, L., Jasin, M., Baer, R., Paull, T.T. *et al.* (2008) A forward chemical genetic screen reveals an inhibitor of the Mre11-Rad50-Nbs1 complex. *Nat. Chem. Biol.*, **4**, 119–125.
46. Hanahan, D. and Weinberg, R.A. (2011) Hallmarks of cancer: the next generation. *Cell*, **144**, 646–674.